View metadata, citation and similar papers at core.ac.uk

brought to you by CORE

provided by Sheffield Hallam University Research Archive

Sheffield Hallam University

Calculation of the Shunt Resistance across the Absorber Layer of Hydrogenated Amorphous Silicon Photovoltaic Cells

AL TARABSHEH, Anas and AKMAL, Muhammad <http://orcid.org/0000-0002-3498-4146>

Available from Sheffield Hallam University Research Archive (SHURA) at:

http://shura.shu.ac.uk/25011/

This document is the author deposited version. You are advised to consult the publisher's version if you wish to cite from it.

Published version

AL TARABSHEH, Anas and AKMAL, Muhammad (2019). Calculation of the Shunt Resistance across the Absorber Layer of Hydrogenated Amorphous Silicon Photovoltaic Cells. In: 2019 6th International Conference on Electrical and Electronics Engineering (ICEEE). IEEE.

Copyright and re-use policy

See http://shura.shu.ac.uk/information.html

Sheffield Hallam University Research Archive
http://shura.shu.ac.uk

Calculation of the Shunt Resistance across the Absorber Layer of Hydrogenated Amorphous Silicon Photovoltaic Cells

A. Al Tarabsheh [1,2], M. Akmal [3]
[1]Electrical and Computer Engineering Dept., Abu Dhabi University, 59911 Abu Dhabi, UAE
[2]Electrical Engineering Dept., The Hashemite University, 13115 Zarqa, Jordan
[3]Electrical and Power Engineering Dept., Sheffield Hallam University, Sheffield S1, UK; m.akmal@shu.ac.uk
Corresponding author:anas.altarabsheh@adu.ac.ae

***Abstract*—In contrast to the existing conventional models, that describe the shunt resistance of hydrogenated amorphous silicon as a uniform resistance a cross the absorber layer (*i*-layer), our paper calculates the shunt resistance of a-Si:H PV cells as a function of the location across the *i*-layer resulting in a more detailed description of the shunt resistance. The photo-generation of the electron-hole pairs depend the photons' wavelength values and the potential across the PV cell. The shunt resistance exists because of the current leakage between the front- and back-contact layers within the *i*-layer. The electric current of the electrons and holes is calculated, in this paper, by solving the Poisson, continuity, and transport equations at each location within the *i*-layer for wide range potential values. In this article, the contribution of electrons and holes on the shunt leakage is calculated for each carrier independently by separating the current density/voltage (*J/V*) curves of the electrons and of the holes at each location within the *i*-layer. This work proves that the effective value of the location-dependent shunt resistances due to the electrons and holes equals the effective shunt resistance of the PV cell calculated from the total *J/V*.**

***Keywords*—**Shunt resistance; hydrogenated amorphous silicon; continuity and transport equations; and current density voltage characteristics.

1. Introduction

The development of hydrogenated amorphous silicon (a-Si:H) photovoltaic (PV) cells has been improved due to concurrent advances in the materials and the novel cell designs. The main advantages of a-Si:H PV cells are: their fabrication cost is low compared to that of crystalline PV cells, their enhanced power output under high temperature conditions because of their small temperature coefficients, their great absorption of diffuse radiation, and their low deposition temperatures [1] needed for flexible plastic substrates.

In a-Si:H semiconductors, slight variations exist in the bond lengths and bond angles between the atoms. The elementary defects (dangling bonds) are the coordination defects when an atom has too many or too few bonds. The a-Si:H materials have high absorption constant due to the random nature of the atomic ordering, therefore they behave like direct bandgap semiconductors [2]. The absence of long-range order in a-Si:H materials broadens the distribution of localized states in the gap that determine many of the optoelectronic properties. The existence of localized defects leads to the charge leakage within the intrinsic region, *i*-layer, between the front and back contacts which in turn makes the *i*-layer electrically active [3].

The PV cell performance is determined mainly by: open circuit voltage (V_{oc}), fill factor (FF), and efficiency (η) which degrade with the increase of the shunt leakage current (i.e the decrease of the shunt resistance R_{sh}) [4]. Figure 1 shows the degradation of the a-Si:H PV cell performance as a function of the decrease in the shunt resistance R_{sh} values. The increase in the shunt leakage current reduces the open circuit voltage, the fill factor, and the efficiency.

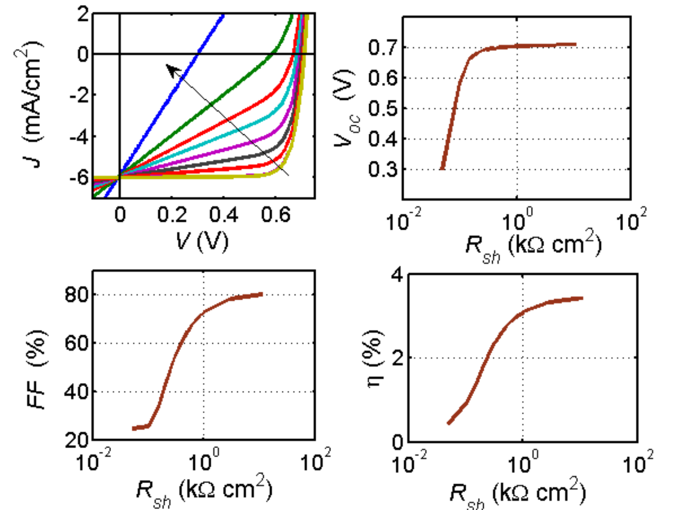

Figure 1: Effect of decreasing the shunt resistance R_{sh} on (a) the current density characteristics (the direction of the arrow indicates an decrease of R_{sh}), (b) the open circuit voltage V_{oc} (c) the fill factor FF, and (d) the efficiency η of the PV cell.

The Current density voltage (*J/V*) characteristics measurement is a primary characterization tool for a-Si:H PV cells to determine their electrical parameters. The general equation for the *J/V* characteristics is:

$$J = J_0\left(\exp\left(\frac{V - JR_s}{n_{id}V_t}\right) - 1\right) + \left(\frac{V - JR_s}{R_{sh}}\right) - J_{ph} \quad (1)$$

Where V is the applied voltage to, or created voltage from, the PV cell, J is the current density, V_t (equals $25.9mV$ at room temperature) is the thermal voltage, n_{id} is the diode ideality factor, J_{ph} is the photocurrent density, R_s is the series resistance, R_{sh} is the shunt resistance[5], and J_0 is the reverse saturation current density. The term $(V - JR_s)/R_{sh}$ of (1) represents the leakage shunt current density through the shunt resistance which can be evaluated from slope of J versus V at the current reading around the point $V = 0V$ [6-9]. The physical origins of the shunt leakage current in a-Si:H PV cells are due to the lateral drift currents and the microscopic pinholes that could form in the *i*-layer during the deposition processes [10].

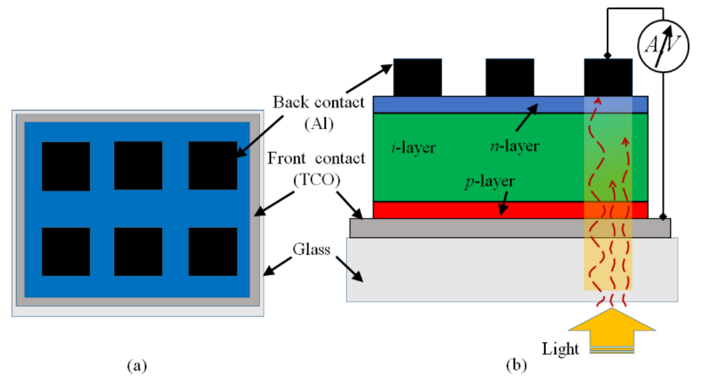

Figure 2: Structure of *p-i-n* a-Si:H PV cell illuminated from the *p*-layer side; (a) top view, (b) cross-section view. The transparent conducting oxide (TCO) has to have good electrical and optical characteristics.

2. Analysis

In this work, the studied cells are a-Si:H PV cells which are fabricated at the Institute for Photovoltaics- University of Stuttgart by the plasma enhanced chemical vapor deposition (PECVD) [11] with a radio frequency of 13.56 MHz at an already TCO-coated glass at a deposition temperature of 180 °C. The area of each cell is 0.3 cm^2. The optical parameters, such as the optical bandgap and film thickness, are determined from ellipsometry measurements [12]. The cells have *p-i-n* structure where the *p*-layer is first deposited on the top of the transparent conducting oxide (TCO). The *p*-layer has a high band gap and a high conductivity compared to the other layers. This results in a higher built-in potential and allows more illumination to penetrate to the *i*-layer. Therefore, it improves the short circuit current density and open circuit voltage [13].

The thickness values of the *p*-layer and the *i*-layer are 27 nm and 120 nm, respectively. The *i*-layer is considered the effective layer of the cell where the absorption of the carriers has to be as maximum as possible. The *n*-layer is deposited just after the *i*-layer and then followed by the sputtering of Aluminum (Al) contact. Figure 2 shows the top and cross section views of an a-Si:H PV cell where the first semiconductor material deposited is the *p*-layer. The TCO material has to be a good transparent and conductive material in order to maximize the photons reaching the *p*-layer and then collect the photogenerated carriers out of the cell. The resulting geometry is called *p-i-n* where the light penetrates first the *p*-layer region. This geometry sets up an electric field, extends between the *p*-layer and *n*-layer regions across the *i*-layer, which separates the absorbed photogenerated electron-hole pairs in order to be collected at the *p*-layer and *n*-layer, respectively.

To analyze the photogenerated current of the a-Si:H PV cell, the optical properties of the *p*- and the *i*-layers are taken into consideration. The a-Si:H films have high optical absorption constant in the visible range of the solar spectrum [14] since the photon energies within this range are absorbed by direct transition of the electrons from the occupied states in the valence band to the empty states of the conduction band [15]. This characteristic enables the a-Si:H PV cells to completely absorb sun light with thicknesses less than 1 µm. To measure the absorption constant α , an ultraviolet-to-infrared spectrophotometer (Varian Cary-5) is used in the wavelength range between 400 nm and 2000 nm for the two semiconductor layers, fabricated at the Institute for Photovoltaics in the University of Stuttgart, which reflects how much solar energy can be absorbed in the front and absorber layers.

3. Discussion and Results

This paper applies the equations of the model developed by Al Tarabsheh [16] which calculate the current voltage characteristics of a-Si:H PV cells. In this model, the Poisson and continuity equations for both types of carriers (electrons and holes) are solved. In more details, the continuity equations for the minority carriers are solved, then this solution is substituted into the equations for majority carriers. The solutions of the two second-order differential equations result in a set of algebraic equations which are finally solved by a matrix inversion. Thus, this work ends up with three curves of the current voltage characteristics for; electrons, holes, and for the total carriers.

The parasitic resistances in PV cells are shunt resistance R_{sh} and series resistance R_s . In the forward current voltage characteristic, the impact of R_{sh} is an undesired current excess at low biases, also known as shunt leakage, while R_s limits the current at high voltages. The increase of the shunt leakage current (i.e, lowering the value of R_{sh}) [17,18] affects the current values in the range between 0 V and the voltage at maximum power point, and diminishes the fill factor and the efficiency of the PV cells as shown in Figure 1. The increase of R_s reduces

significantly the current at voltage values higher than the voltage at maximum power point [19]. From each curve, the shunt resistances are determined from the slope dV/dJ near short-circuit conditions (i.e $V = 0V$). As a result, a shunt resistance due to the electrons $R_{sh,n}$, a shunt resistance due to the holes $R_{sh,p}$, and an effective shunt resistance due to the both carriers R_{sh} are evaluated separately.

The photogeneration rate $G(\lambda, x)$ within the *i*-layer depends on the incoming AM 1.5 solar spectrum $N_{ph}(\lambda)$ and the absorption constant α [20] as $G(\lambda, x) = \alpha(\lambda) N_{ph}(\lambda) \exp(-\alpha(\lambda) x)$. The continuity equation for the electrons (similar equations can be applied for holes as well) [16] can be expressed as:

$$\frac{d^2 n(x,\lambda)}{dx^2} + E\frac{\mu_n}{D_n}\frac{dn(x,\lambda)}{dx} - \frac{n(x,\lambda)}{D_n \tau_n} = -\left[\frac{N_D}{D_n \tau_n} e^{\frac{V_{bi} W}{V_t (x-W)}} + \frac{G(x,\lambda)}{D_n}\right] \quad (2)$$

and

$$E\mu_p \frac{dp(x,\lambda)}{dx} - D_p \frac{d^2 p(x,\lambda)}{dx^2} = -\frac{n(x,\lambda) - n_0(x,\lambda)}{\tau_n} + G(x,\lambda) \quad (3)$$

Where x is the distance from the reference (*p*-layer), E is the electric field within the i-layer, μ_n is the electron mobility, τ_n is the electron lifetime, μ_p is the hole mobility, τ_p is the hole lifetime, D_n is the diffusion constant of the electrons, D_p is the diffusion constant of the holes, N_D is the concentration of the donors, N_A is the concentration of the acceptors, V_{bi} is the built-in voltage, V_t is the thermal voltage, W is the width of the *i*-layer, and n_0 is the concentration of the electrons at thermal equilibrium.

Figure 3 depicts the total carrier concentrations of holes $p(x)$ and electrons $n(x)$ in the *i*-layer of the tested *p-i-n* PV cell at different applied voltages. The higher the applied voltage the higher the concentrations of carriers will be.

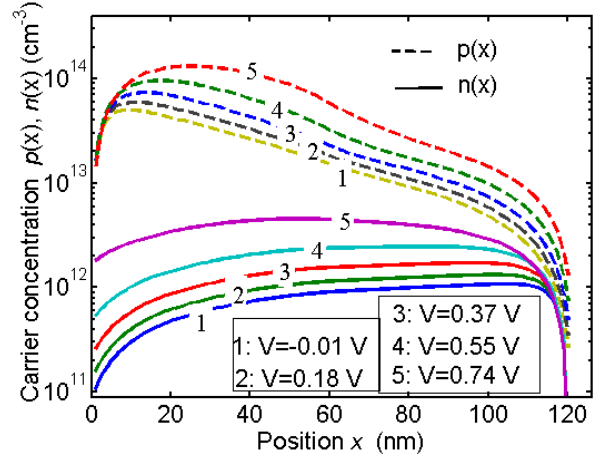

Figure 3: Calculated total carrier concentrations of holes $p(x)$ (dashed lines) and electrons $n(x)$ (solid lines) in the absorber layer of the tested *p-i-n* PV cell at different applied voltage values. The higher the applied voltage the higher the concentrations of the carriers will be.

The calculation of the current density of electrons J_n (similar calculation applies for current density of holes J_p as well) for the *p-i-n* PV cell comes from the solutions of the diffusion and the drift equations [21] as in (4). Both current densities will be voltage- and position-dependent.

$$J_n(x) = q\mu_n n(x)E + qD_n \frac{dn(x)}{dx} \quad (4.a)$$

$$J_p(x) = q\mu_p p(x)E - qD_p \frac{dp(x)}{dx} \quad (4.b)$$

The summation of the electron and hole current densities gives the total current density J. The analytical model developed by Al Tarabsheh is applied to simulate a measured illuminated current voltage J/V-characteristics of the fabricated a-Si:H PV cells which are deposited on Asahi-U coated glass superstrates. Fitting the measured *J/V*-characteristics by the analytical model as shown in Figure 4 where the analytical model well reproduces the measured *J/V*-characteristics of the a-Si:H PV cell. The structure *p-i-n* is preferred since, according to Beer's absorption law, most of the incident light is absorbed close to the front of the illuminated layer [22], and the mobility-lifetime product $\mu_p \tau_p$ value of holes in a-Si:H cells is less than $\mu_n \tau_n$ for electrons [23]. Figure 4 shows the current density-voltage *J/V*-characteristics of the tested *p-i-n* a-Si:H PV cell where the simulation (solid line) agrees with measurement (symbols) data. The optimum fitting parameters used are: $N_D = 2\times10^{16} cm^{-3}$, $N_A = 1\times10^{15} cm^{-3}$, $\mu_n = 0.55 cm^2V^{-1}s^{-1}$, $\mu_p = 0.01 cm^2V^{-1}s^{-1}$, $\tau_n = 10^{-6} s$, and $\tau_p = 10^{-8} s$.

Since the analytical model expresses the total current density J of the measured a-Si:H PV cells, then the calculations of all quantities in the analytical model will be

accepted.

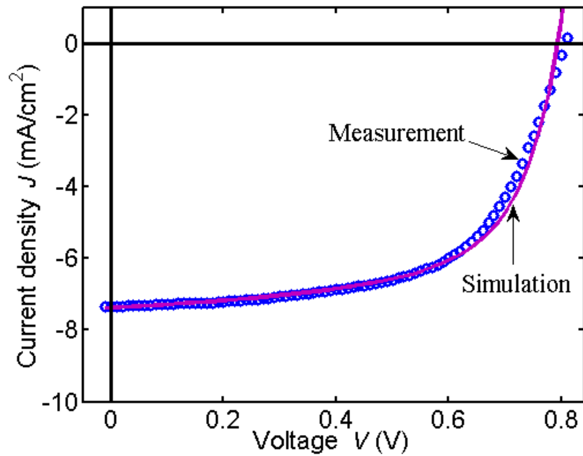

Figure 4: Current density-voltage *J/V*-characteristics of the tested *p-i-n* a-Si:H PV cell. The values of the measured *J/V*-characteristics (symbols) are simulated with the analytical model (solid line) by the following parameters: $N_D = 2\times10^{16} cm^{-3}$, $N_A = 1\times10^{15} cm^{-3}$, $\mu_n = 0.55 cm^2V^{-1}s^{-1}$, $\mu_p = 0.01 cm^2V^{-1}s^{-1}$, $\tau_n = 10^{-6} s$, and $\tau_p = 10^{-8} s$

This paper calculates the contributions of the electron and hole current densities, J_n and J_p, respectively, at each location within the *i*-layer at different applied voltage values. The shunt resistance R_{sh} reflects the leakage of the carries between the front and back contacts within the absorber layer. Since the model calculates J_n and J_p separately then there will be two leakage currents due to the electrons and the holes resulting in two shunt resistances due to the electrons and the holes, $R_{sh,n}$ and $R_{sh,p}$ respectively. The total (effective) shunt resistance R_{sh} is calculated from the total current density *J*.

The shunt resistance is calculated by a linear fit for the *J/V*-characteristics around $V = 0\,\text{V}$ [24]. The shunt resistances $R_{sh,n}$, $R_{sh,p}$, and R_{sh} are calculated and depicted in Figure 5 where the constant values of R_{sh} match very well the equivalent parallel values of $R_{sh,n} // R_{sh,p}$. The conclusion of this part is that the effective shunt resistance equals the inverse sum of the inverse values of the corresponding shunt resistances of the carriers.

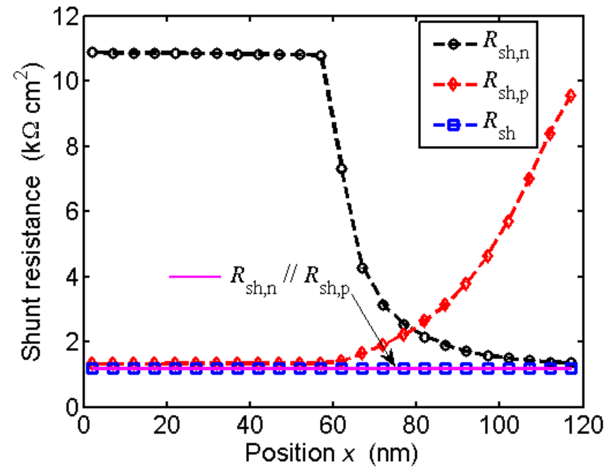

Figure 5: Shunt resistance due to electrons (circles) $R_{sh,n}$, holes (diamonds) $R_{sh,p}$, total carries (squares) R_{sh}, and the parallel value $R_{sh,n} // R_{sh,p}$ (solid line).

This paper also finds that low carrier mobilities cause an apparent shunt resistance. Since the concept of the shunt resistance is frequently used in the literature to account for the non-zero slope of the curve at short-circuit conditions, the existing simulations reveal that non-zero slopes of the *J/V* curves are inevitable consequence of low values of the carrier mobilities. Values for the effective shunt resistance deduced from the simulated *J/V* curves change over a wide range, depending strongly on mobility which agrees with the work of Wuerfel [25].

4. Conclusion

This paper described the spatial variation of the shunt resistance of a-Si:H PV cells at each position within the *i*-layer. The current density voltage *J/V* curves of each type of the charge carriers were calculated by solving the Poisson, continuity, and transport equations at each location within the *i*-layer. Since the *J/V* curves of the two carriers vary with along with the *i*-layer, the shunt leakage current of each carrier will vary accordingly. As a result, this paper found that the parallel equivalent value of the location-dependent shunt resistances due to the electrons and holes equals the effective shunt resistance of the PV cell calculated from the total *J/V* characteristic. This results in that the shunt resistance used in the equivalent circuit of PV cells is composed of two parallel connected shunt resistances; one due to electrons and one due the holes. Also, this paper showed that enhancing the carriers' mobility values decreases the shunt leakage current in the bulk of the PV cell.

5. Acknowledgment

The authors would like to acknowledge the Institute for Photovoltaics at University of Stuttgart-Germany for the fabrication of hydrogenated amorphous silicon photovoltaic cells and Abu Dhabi University for funding this work under the grant "19200212".

6. REFERENCES

1. Ball J. M., Lee M. M., Hey A., Snaith H. J., Low-temperature processed meso-super structured to thin-film perovskite solar cells, DOI: 10.1039/C3EE40810H, Energy Environ. Sci., Vol. 6, pp. 1739-1743, 2013.
2. Derkacs D., Lim S. H., Matheu P., Mar W., and Yub E. T., Improved performance of hydrogenated amorphous silicon solar cells via scattering from surface plasmon polaritons in nearby metallic nanoparticles, APPLIED PHYSICS LETTERS 89, 093103, 2006.
3. Breitenstein O., Rakotoniaina J.P., Al Rifai M.H., Werner M., Shunt type in crystalline silicon solar cells, Progress in Photovoltaics: Research and Applications 12 (2004) 529–538
4. Tuyen N., Fujita G., PV-Active Power Filter Combination Supplies Power to Nonlinear Load and Compensates Utility Current, IEEE Power and Energy Technology Systems Journal, Vol.2, No. 1, 2015.
5. Zahedi A., Maximizing solar PV energy penetration using energy storage technology , Renewable and Sustainable Energy Reviews , Volume 15, Issue 1, 2011, pp. 866-870.
6. Werner J. H, Schottky barrier and pn-junction I/V plots—Small signal evaluation, Applied Physics A: Materials Science & Processing, Vol. 47 (3), pp. 291-300, 1988.
7. K. Bouzidi K., Chegaar M. , Bouhemadou A., Solar cells parameters evaluation considering the series and shunt resistance, Solar Energy Materials and Solar Cells, Vol. 91, Issue 18, pp. 1647–1651, 2007..
8. Somasundaran P., Gupta R., Influence of local shunting on the electrical performance in industrial Silicon solar cells, Solar Energy, Vol. 139, pp. 581–590, 2016.
9. Cotfasa D.T., Cotfasa P.A., Kaplanisb S., Methods and techniques to determine the dynamic parameters of solar cells: Review, Renewable and Sustainable Energy Reviews, Vol. 61, pp. 213–221, 2016.
10. Dongaonkar S., Servaites J. D., Ford G. M., Loser S., Moore J., Gelfand R. M., Mohseni H., Hillhouse H. W., Agrawal R., Ratner M. A., T. J. Marks, Lundstrom M. S., and Alam M. A., Universality of non-Ohmic shunt leakage in thin-film solar cells, Journal of Applied Physics 108, 124509, 2010.
11. Lieberman M. A., Lichtenberg A. J., Principles of Plasma Discharges and Materials Processing, John Wiley, page 514, 1994.
12. Kim S., Jin-Won Chung, H. Lee, Park J., Heo, Heon-Min Lee, Remarkable progress in thin-film silicon solar cells using high-efficiency triple-junction technology, Solar Energy Materials & Solar Cells, Vol. 119, pp. 26–35, 2013.
13. C.-T. Li, Hsieh F., Wang L., Performance improvement of *p*-type silicon solar cells with thin silicon films deposited by low pressure chemical vapor deposition method. Sol Energy 88 (0), 104–109, 2013.
14. Namakwa Y., Thin-Film Solar Cells Next Generation Photovoltaics and Its Applications, Springer, pp.46, 2004.
15. Al Tarabsheh A., Hydrogenated amorphous silicon Based Solar Cells, Ph.D. thesis, Stuttgart Universität, 2007.
16. Al Tarabsheh A., Description of the Ideality Factor of a-Si:H Photovoltaic Cells Under Different Illumination Intensity Levels, Journal of Renewable and Sustainable Energy, DOI: 10.1063/1.4918286, Vol. 7, Issue, 2, 2015.
17. Acharya P., Shaikh M. N., Jha S. K., A. P. Papadakis, Electrical Modelling Of a Photovoltaic Module, Engineering and Industry Series Volume Power Systems, Energy Markets and Renewable Energy Sources in South-Eastern Europe, 2016.
18. Fortes M., Comesan E. , Rodriguez J.A., Otero P., Garcia-Loureiro A.J., Impact of series and shunt resistances in amorphous silicon thin film solar cells, Solar Energy ,Vol. 100, pp.114–123, 2014.
19. Meral M., Dinçer F., A review of the factors affecting operation and efficiency of photovoltaic based electricity generation systems, Renewable and Sustainable Energy Reviews , Volume 15, Issue 5, 2011, pp. 2176-2184,
20. U. Wurfel, Andres Cuevas, P. Wurfel, Charge Carrier Separation in Solar Cells, IEEE Journal of Photovoltaics, Vol. 5, No. 1, 2015.
21. Taretto K., New explicit current/voltage equation for *p-i-n* solar cells including interface potential drops and drift/ diffusion transport, DOI: 10.1002/pip.2325, Progress in Photovoltaics: Research and Applications, 2012.
22. Wieder S., Hydrogenated amorphous silicon solar cells: comparison of *p-i-n* and *n-i-p* structures with zinc-oxide front contact, Ph.D. thesis, Forschungszentrum Juelich, pp. 9, 1999.
23. Álvarez-Macías C., Escobar-Carrasquilla J. D., Dutt A., Mon-Pérez E., González L., and Santana G., Development of Optimal Nanocrystalline Absorption Layer for Thin Film Silicon Solar Cell Applications, Nano, Vol. 12, No. 11, 2017.
24. Lineykin S., Averbukh M., Kuperman A., An improved approach to extract the single-diode equivalent circuit parameters of a photovoltaic cell/panel, Vol. 30, pp. 282–289, 2014.
25. Wuerfel U., Neher D., Spies A., Albrecht S., Impact of charge transport on current–voltage characteristics and power-conversion efficiency of organic solar cells, Nature Communications Vol. 6, DOI: 10.1038/ncomms795, Article number: 6951, 2015.